7 Appendix

7.1 Compensated Tracking Error Dynamics

The dynamics of the compensated tracking errors are derived in three different cases.

(1) For $i = 1$

$$\begin{aligned}\dot{\bar{x}}_1 = &-k_1\bar{x}_1 - \beta_{f_1} + u_{s_1} + (f_1 - \hat{f}_1) - \beta_{g_1}x_2 \\ &+(g_1^o + \hat{g}_1 + \beta_{g_1})\bar{x}_2 + (g_1 - \hat{g}_1)x_2. \end{aligned} \quad (32)$$

(2) For $1 < i < n$:

$$\begin{aligned}\dot{\bar{x}}_i = &-k_i\bar{x}_i - \beta_{f_i} + u_{s_i} + (f_i - \hat{f}_i) \\ &-(g_{i-1}^o + \hat{g}_{i-1} + \beta_{g_{i-1}})\bar{x}_{i-1} - \beta_{g_i}x_{i+1} \\ &+(g_i^o + \hat{g}_i + \beta_{g_i})\bar{x}_{i+1} + (g_i - \hat{g}_i)x_{i+1}. \end{aligned} \quad (33)$$

(3) For $i = n$ ($\bar{x}_n = \tilde{x}_n$):

$$\begin{aligned}\dot{\bar{x}}_n = &-k_n\bar{x}_n - (g_{n-1}^o + \hat{g}_{n-1} + \beta_{g_n-1})\bar{x}_{n-1} - \beta_{f_n} \\ &+(f_n - \hat{f}_n) - \beta_{g_n}u_{ad} + (g_n - \hat{g}_n)u_{ad} \\ &+(g_n^o + g_n)u_{s_n}. \end{aligned} \quad (34)$$

7.2 Command Filtering

For each $i \in [2, n]$, the signal x_{ic} is required for eqn. (3) and its derivative $\dot{x}_{ic}$ is required for calculating u_{a_i} (see eqns. (6) and (10)). They are defined by the following procedure (Farrell *et al.* 2004, Farrell & Polycarpou 2006).

(1) For i=1,. . . ,n-1, define

$$x_{i+1,c}^0 = \alpha_i - \xi_{i+1}. \quad (35)$$

The signals $x_{i+1,c}$ and $\dot{x}_{i+1,c}$ are defined by

$$\dot{x}_{i+1,c} = -K_{i+1}(x_{i+1,c} - x_{i+1,c}^0) \quad (36)$$

with $K_{i+1} > k_{i+1}$ being a designer specified constant and $x_{i+1,c}(0) = \alpha_i(0)$. Since the filter of (36) is being used as a means to compute $x_{i+1,c}$ and $\dot{x}_{i+1,c}$ without differentiation, the designer would typically select $K_{i+1} \gg k_{i+1}$ so that $x_{i+1,c}$ accurately tracks $x_{i+1,c}^0$ over the bandwidth of $x_{i+1,c}^0$. Since (36) is a stable linear filter, $x_{i+1,c}$ and $\dot{x}_{i+1,c}$ will be bounded if the input $x_{i+1,c}^0$ is bounded.

(2) For i=1,. . . ,n-1, define

$$\dot{\xi}_i = -k_i\xi_i + (g_i^o + \hat{g}_i + \beta_{g_i})(x_{i+1,c} - x_{i+1,c}^0) \quad (37)$$

with $\xi_i(0) = 0$.
This is a stable low pass filter. Its input is the product of $(g_i^o + \hat{g}_i + \beta_{g_i})$ which we will prove to be bounded and $(x_{i+1,c} - x_{i+1,c}^0)$ which is small. For $x_{i+1,c}, x_{i+1,c}^0 \in \mathcal{D}$ we always have that $|(x_{i+1,c} - x_{i+1,c}^0| < 2\rho(\mathcal{D})$ where $\rho(\mathcal{D}) = \max_{x_1,x_2\in\mathcal{D}} \|x_1 - x_2\|$ is the diameter of set $\mathcal{D}$. For any x, each ξ_i is bounded by $\bar{b}_\xi$, i.e., $|\xi_i| \le \bar{b}_\xi$, where

$$\bar{b}_\xi = \frac{2\rho(\mathcal{D})}{\underline{k}} \max_i \Big[\sup_{\forall t} (|g_i^o + \hat{g}_i + \beta_{g_i}|) \Big] \quad (38)$$

with $\underline{k} = \min_i\{k_i\}$.
For completeness, the signal $\xi_n = 0$.

7.3 Sliding Mode

For $x(t) \notin \mathcal{D}$, we implement sliding components within the control design to return the state x to the approximation region $\mathcal{D}$ in finite time. The following assumption is required for the sliding mode design.

Assumption 4 *For $i = 1, \ldots, n$, there exist known upper bounds on unknown functions $|f_i(x)|$ and $|g_i(x)|$ such that $|f_i(x)| \le \bar{b}_{f_i}$ and $|g_i(x)| \le \bar{b}_{g_i}$ for any $x(t) \in \Re^n - \mathcal{D}$.*

Note that if constants $\bar{b}_{f_i}$ and $\bar{b}_{g_i}$ are not known, then they could be estimated using the methods suggested in (Polycarpou 1996). We do not present such an adaptive bounding approach herein for $x \notin \mathcal{D}$ as that portion of the state space is not the main topic of this article. Note also that the approach extends directly to more general (e.g., linear or quadratic growth) bounds than the constant bounds assumed herein.

The $u_{s_i}(t)$ terms in eqns. (5–6) are defined as

$$u_{s_i}(t) = -r_i(t)sign(\bar{x}_i) \quad (39)$$

and the gain $r_i(t)$ is given by

$$r_i(t) = \begin{cases} 0, & \text{when } x \in \mathcal{D} \\ \bar{b}_{f_i} + \bar{b}_{g_i}|x_{i+1}|, & \text{when } x \notin \mathcal{D} \end{cases} \quad (40)$$

where $\bar{b}_{f_i}, \bar{b}_{g_i}$ are known bounds on $|f_i(x)|$ and $|g_i(x)|$ satisfying the Assumption 4 for $x \notin \mathcal{D}$.

The sliding component u_{s_n} is defined as

$$u_{s_n} = -r_n(t)sign(\bar{x}_n) \quad (41)$$

$$r_n(t) = \begin{cases} 0, & \text{when } x \in \mathcal{D} \\ \frac{\bar{b}_{f_n} + \bar{b}_{g_n}|u_{ad}|}{g_n^o + g_l}, & \text{when } x \notin \mathcal{D}. \end{cases} \quad (42)$$

where $\bar{b}_{f_n}$ and $\bar{b}_{g_n}$ are known bounds on $|f_n(x)|$ and $|g_n(x)|$ satisfying the Assumption 4 for $x \notin \mathcal{D}$.

The main objective of this section is to demonstrate that the definitions of $u_{si}, 1 \le i \le (n-1)$ in eqns. (39–40) and

u_{sn} in eqns. (41–42) ensure that any initial conditions outside $\mathcal{D}$ will return to region $\mathcal{D}$ in finite time.

To analyze performance for $x \notin \mathcal{D}$, we consider the Lyapunov function

$$\bar{V} = \frac{1}{2}\sum_{i=1}^{n} \bar{x}_i^2. \tag{43}$$

Using $\beta_{f_i} = \beta_{g_i} = 0$, $\hat{f}_i(x) = 0$, and $\hat{g}_i(x) = g_l$ for $x \notin \mathcal{D}$ to simplify compensated tracking error dynamics in eqns. (32 - 34) and applying the sliding control of (39) and (41), we obtain the derivative of $\bar{V}$ defined in eqn. (43) as

$$\begin{aligned}\frac{d\bar{V}}{dt} \leq & -\sum_{i=1}^{n} k_i \bar{x}_i^2 + \sum_{i=1}^{n-1} |\bar{x}_i|\,(-r_i + |d_i|) \\ & + |\bar{x}_n|\Big(- (g_n^o + g_n) r_n + |d_n|\Big)\end{aligned} \tag{44}$$

where we let

$$d_i = \begin{cases} f_i + (g_i - g_l)x_{i+1}, \text{ for } 1 \leq i < n \\ f_n + (g_n - g_l)u_{ad}, \text{ for } i = n. \end{cases}$$

Since the sliding gains of (40) and (42) yield, for $i < n$

$$|d_i| \leq |f_i| + (g_i - g_l)|x_{i+1}| \leq \bar{b}_{f_i} + \bar{b}_{g_i}|x_{i+1}| = r_i,$$

and, for $i = n$

$$|d_n| \leq |f_n| + (g_n - g_l)|u_{ad}| \leq (g_n^o + g_n) r_n,$$

the last two terms on the right of (44) are non-positive. Then, we attain

$$\frac{d\bar{V}}{dt} \leq -\sum_{i=1}^{n} k_i \bar{x}_i^2 < -\underline{k}\bar{V} \tag{45}$$

$$\bar{V}(t) \leq e^{-\underline{k}t}\bar{V}(0), \text{ for any } t \geq 0. \tag{46}$$

Therefore, there exists a finite T_2 such that for any $t > T_2$, $\bar{V}(t) < \frac{\gamma^2}{8}$ which implies that $\|\bar{x}(t)\| < \frac{\gamma}{2}$. In addition, for $x \notin \mathcal{D}$, if $x_{i+1,c}, x_{i+1,c}^0$ are within a compact region $\mathcal{B}$, then $|\xi_i| < \bar{b}_\xi$ where $\bar{b}_\xi = \frac{2\rho(\mathcal{B})}{\underline{k}}(g_i^o + g_l)$ by methods similar to those used to derive (38). Therefore, we can attain $\|\xi(t)\| < \frac{\gamma}{2}$ for $x \notin \mathcal{D}$ by choosing $\frac{\gamma}{2} > \bar{b}_\xi$. Therefore, for $t > T_2$,

$$\|\tilde{x}(t)\| \leq \|\bar{x}(t)\| + \|\xi(t)\| < \gamma$$

which implies that x returns to within $\mathcal{D}$ in finite time. The state in $\mathcal{D}$ may leave that region, but will return to $\mathcal{D}$ in finite time.

7.4 $\bar{x}$ Modification

As we state in Section 5.1, the main drawback of the standard σ-modification is that it causes the parameter estimates to drift towards certain design vectors. This can occur for θ_i either when $x \notin S_i$ or when $x \in S_i$ and $\|\bar{x}\|$ is small. In Section 5.1 the first issue was addressed by localization of the σ-modification term. The second issue can be addressed by a localized $\bar{x}$-modification as presented in this section.

The localized $\bar{x}$-modification terms are defined as,

$$Q_{f_i} = -\sigma_{f_i} \ \|\bar{x}\| R_{f_i}(\theta_{f_i} - \theta_{f_i}^0) \tag{47}$$

$$Q_{g_i} = -\sigma_{g_i} \ \|\bar{x}\| R_{g_i}(\theta_{g_i} - \theta_{g_i}^0) \tag{48}$$

$$Q_{\Psi f_i} = -\sigma_{\Psi f_i}\|\bar{x}\| R_{f_i}(\Psi_{f_i} - \Psi_{f_i}^0) \tag{49}$$

$$Q_{\Psi g_i} = -\sigma_{\Psi g_i}\|\bar{x}\| R_{g_i}(\Psi_{g_i} - \Psi_{g_i}^0) \tag{50}$$

for $i = 1, \ldots, n$. For consistancy, we have used the same design parameter notation as in the σ-modification approach.

Substituting the Q terms defined in (47–50) into (22), we obtain the derivative of $V(t)$ as

$$\dot{V} \leq -\underline{k}\|\bar{x}\|^2 + \bar{d} + \|\bar{x}\|\rho_1 \tag{51}$$

where ρ_1 is defined in eqn. (29). In eqn. (51), using the inequality $pq \leq \alpha^2 p^2 + \frac{1}{4\alpha^2}q^2$ with $\alpha^2 = \frac{\underline{k}}{2}$, we obtain

$$\dot{V} \leq -\frac{1}{2}\underline{k}\|\bar{x}\|^2 + \bar{d} + \rho_2 \tag{52}$$

where ρ_2 is a positive constant given by

$$\rho_2 = \frac{1}{2\underline{k}}\rho_1^2. \tag{53}$$

Therefore, we can summarize these results in the following theorem.

Theorem 3 *[$\bar{x}$-modification] For the higher order system described by (1)-(2) with the adaptive feedback control law of eqns. (8), (9–10), (41–42), and the parameter adaptation laws of eqns.(13–14) and (15–16) with modification terms defined in (47–50), we have the following stability properties, for $i = 1, \ldots, n$,*

(1) $\bar{x}_i, \tilde{\theta}_{f_i}, \tilde{\theta}_{g_i}, \tilde{\Psi}_{f_i}, \tilde{\Psi}_{g_i} \in \mathcal{L}_\infty$;
(2) $x_i, \theta_{f_i}, \theta_{g_i}, \Psi_{f_i}, \Psi_{g_i} \in \mathcal{L}_\infty$;
(3) $\dot{\bar{x}}_i, \dot{\theta}_{f_i}, \dot{\theta}_{g_i}, \dot{\Psi}_{f_i}, \dot{\Psi}_{g_i} \in \mathcal{L}_\infty$;
(4) $\bar{x}$ is small in the mean square sense, satisfying

$$\int_t^{t+T} \|\bar{x}(\tau)\|_2^2 d\tau \leq \frac{2}{\underline{k}}V(t) + \frac{2}{\underline{k}}(\bar{d} + \rho_2)T. \tag{54}$$

Similar comments about the localized forgetting apply as were stated in the Section 5.1.

7.5 Deadzone

Another means to remove the issue of parameter drift is to include a deadzone in adaptive laws. Implementation of the deadzone requires knowledge of an assumed bound on certain terms as will be discussed below.

For the deadzone approach, the modification terms in eqns. (13–16) are defined as, for $i = 1, \ldots, n$,

$$Q_{f_i} = \begin{cases} 0 & \text{if } \|\bar{x}\| > \sqrt{\frac{\bar{\rho}_3+\mu}{\underline{k}}} \\ -\Phi_{f_i}\bar{x}_i & \text{otherwise,} \end{cases} \tag{55}$$

$$Q_{g_i} = \begin{cases} 0 & \text{if } \|\bar{x}\| > \sqrt{\frac{\bar{\rho}_3+\mu}{\underline{k}}} \\ -\Phi_{g_i}\bar{x}_i x_{i+1} & \text{if } \|\bar{x}\| \le \sqrt{\frac{\bar{\rho}_3+\mu}{\underline{k}}} \text{ and } i < n \\ -\Phi_{g_n}\bar{x}_n u_{ad} & \text{if } \|\bar{x}\| \le \sqrt{\frac{\bar{\rho}_3+\mu}{\underline{k}}} \text{ and } i = n, \end{cases} \tag{56}$$

and

$$Q_{\Psi f_i} = \begin{cases} -\sigma_{\Psi f_i} R_{f_i}(\Psi_{f_i} - \Psi^0_{f_i}) & \text{if } \|\bar{x}\| > \sqrt{\frac{\bar{\rho}_3+\mu}{\underline{k}}} \\ -\Phi_{f_i}\bar{x}_i\omega\left(\frac{\bar{x}_i}{\epsilon}\right) & \text{otherwise,} \end{cases} \tag{57}$$

$$Q_{\Psi g_i} = \begin{cases} -\sigma_{\Psi g_i} R_{g_i}(\Psi_{g_i} - \Psi^0_{g_i}) & \text{if } \|\bar{x}\| > \sqrt{\frac{\bar{\rho}_3+\mu}{\underline{k}}} \\ -\Phi_{g_i}\bar{x}_i x_{i+1}\omega\left(\frac{\bar{x}_i x_{i+1}}{\epsilon}\right) & \text{if } \|\bar{x}\| \le \sqrt{\frac{\bar{\rho}_3+\mu}{\underline{k}}} \\ & \text{and } i < n \\ -\Phi_{g_n}\bar{x}_n u_{ad}\omega\left(\frac{\bar{x}_n u_{an}}{g_l\epsilon}\right) & \text{if } \|\bar{x}\| \le \sqrt{\frac{\bar{\rho}_3+\mu}{\underline{k}}} \\ & \text{and } i = n. \end{cases} \tag{58}$$

The constant $\bar{\rho}_3 > 0$ is a known strict upper bound on $(\bar{d} + \rho_3)$, where $\bar{d}$ is defined in eqn. (23) and

$$\rho_3 = \frac{1}{2}\sum_{i=1}^{n}\Big(\sigma_{\Psi fi}(\Psi^M_{f_i} - \Psi^0_{f_i})^\top R_{f_i}(\Psi^M_{f_i} - \Psi^0_{f_i}) + \sigma_{\Psi gi}(\Psi^M_{g_i} - \Psi^0_{g_i})^\top R_{g_i}(\Psi^M_{g_i} - \Psi^0_{g_i})\Big). \tag{59}$$

The deadzone is in effect for $\|\bar{x}\| \le \sqrt{\frac{\bar{\rho}_3+\mu}{\underline{k}}}$ for some positive design constant $\mu > 0$. For $\|\bar{x}\| > \sqrt{\frac{\bar{\rho}_3+\mu}{\underline{k}}}$, the parameter adaptation laws of θ_{f_i} and $\theta_{g_i}, i = 1, \ldots, n$ do not include any modification terms. When $\|\bar{x}\| \le \sqrt{\frac{\bar{\rho}_3+\mu}{\underline{k}}}$, all parameter updates stop.

We are now ready to present the applicable stability theorem.

Theorem 4 *[Deadzone] Assuming the upper bound $\bar{\rho}_3 > \bar{d} + \rho_3 > 0$ is known, for the higher order system described by (1)-(2) with the adaptive feedback control law of eqns. (8), (9–10), (41–42), and the parameter adaptation laws of eqns.(13–14) and (15–16) with modification terms defined in (55–58), we have the following stability properties, for $i = 1, \ldots, n$,*

(1) $\bar{x}_i, \tilde{\theta}_{f_i}, \tilde{\theta}_{g_i}, \tilde{\Psi}_{f_i}, \tilde{\Psi}_{g_i} \in \mathcal{L}_\infty$;
(2) $x_i, \theta_{f_i}, \theta_{g_i}, \Psi_{f_i}, \Psi_{g_i} \in \mathcal{L}_\infty$;
(3) $\dot{\bar{x}}_i, \dot{\theta}_{f_i}, \dot{\theta}_{g_i}, \dot{\Psi}_{f_i}, \dot{\Psi}_{g_i} \in \mathcal{L}_\infty$;
(4) $\bar{x}$ is small in the mean square sense, satisfying

$$\int_t^{t+T} \|\bar{x}(\tau)\|_2^2 d\tau \le \frac{1}{\underline{k}} V(t) + b_d^2 T \tag{60}$$

where $b_d = \sqrt{\frac{\bar{\rho}_3+\mu}{\underline{k}}}$ is the deadzone width.
(5) $\|\bar{x}\|$ is ultimately bounded by b_d as $t \to \infty$, i.e., the total time for $\|\bar{x}\| > b_d$ is finite.

Assuming that the design constant $\bar{\rho}_3 > 0$ is a strict upper bound on $(\bar{d} + \rho_3)$, the ultimate bound in Item 5 of Theorem 4 has a useful form that allows the designer to either increase $\underline{k}$ or decrease μ or $\bar{\rho}_3$ to decrease the ultimate bound on the tracking error.

A disadvantage of deadzone modification is that the implementation of the deadzone requires knowledge of $(\bar{d} + \rho_3)$ or the upper bound on it over the whole region $\mathcal{D}$. If $\mathcal{D}$ is relatively large, the upper bound $\bar{\rho}_3$ can be conservative, which may result in a large deadzone.

7.6 Numerical Example

For illustrative purposes, consider the second order system given by

$$\dot{x}_1 = sin(x_1 + x_2) + \Big(2 + g_1(x)\Big)x_2 \tag{61}$$

$$\dot{x}_2 = sin(x_2) + \Big(2 + g_2(x)\Big)u. \tag{62}$$

with $g_1(x) = g_2(x) = \frac{1}{20}\Big(x_1^2 + |x_1|\Big)\cos(0.01\pi x_1)$ and $x = [x_1, x_2]^\top$. The system is designed to operate over the region $\mathcal{D} = [-3, 3] \times [-3, 3]$. Note that eqns. (61 – 62) are in the form of (1 – 2). Assume that the known design models is

$$\dot{x}_1 = 2x_2 \tag{63}$$

$$\dot{x}_2 = 2u. \tag{64}$$

where $f_1^o(x) = f_2^o(x) = 0$, $g_1^o(x) = g_2^o(x) = 2$. In this case, the unknown model errors are $f_1(x) = sin(x_1+x_2)$, $f_2(x) = sin(x_2)$, $g_1(x)$ and $g_2(x)$. Each of these unknown functions will be adaptively approximated during operation.

The reference trajectory $x_d(t)$ and its derivative $\dot{x}_d(t)$ are generated as the output of a second order, unity DC gain, low-pass prefilter given by

$$\dot{z}_1 = z_2$$
$$\dot{z}_2 = a_1 \left[sat\Big(a_2(sat(r) - z_1) \Big) - z_2 \right]$$
$$\begin{bmatrix} x_d \\ \dot{x}_d \end{bmatrix} = \begin{bmatrix} 1 & 0 \\ 0 & 1 \end{bmatrix} \begin{bmatrix} z_1 \\ z_2 \end{bmatrix}$$

where the two $sat(\cdot)$ functions are included to limit the input magnitude and rate such that $(x_d, \dot{x}_d) \in \mathcal{D}$ for any $t > 0$. In our simulations, we select $a_1 = 2\zeta\omega_n$ and $a_2 = \frac{\omega_n^2}{2\zeta\omega_n}$ with $\zeta = 0.9$ and $\omega_n = 5$ such that, in the absence of magnitude and rate saturation, the transfer functions are

$$\frac{x_d^{(i)}(s)}{r(s)} = \frac{\omega_n^2 s^i}{s^2 + 2\zeta\omega_n s + \omega_n^2}, \; i = 0, 1$$

which are Bounded-Input-Bounded-Output (BIBO) stable. As long as $r(t)$ is bounded, we obtain continuous, bounded signals x_d and $\dot{x}_d$ that will be used in the computation of $x_{2c}^0(t)$. Theoretically, the input to the prefilter $r(t)$ can be any bounded signal. For the purpose of this simulation we select $r(t) = 3sin(0.2\pi t)$.

For approximation of f_1, g_1, f_2 and g_2, we use the same vector of basis functions $\Phi(x) = [\phi_1(x), \ldots, \phi_N(x)]^\top$ for all function approximations. The basis functions $\phi_k(x), k = 1, \ldots, N$ are the normalized biquadratic kernels:

$$\phi_k(x) = \begin{cases} \left(1 - R^2\right)^2, & \text{if } R < 1 \\ 0, & \text{otherwise.} \end{cases} \tag{65}$$

where

$$R = \left\| \frac{|x_1 - c_{k,1}|}{\mu_{k,1}}, \frac{|x_2 - c_{k,2}|}{\mu_{k,2}} \right\|_\infty ;$$

$c_k = [c_{k,1}, c_{k,2}]^\top$ is the center location of the k-th basis function; and, $\mu_{k,1}$ and $\mu_{k,2}$ are the constant radii of the region of support in the x_1 and x_2 directions, respectively. For both x_1 and x_2, the centers are allocated 0.3 units apart with $\mu_{k,1} = \mu_{k,2} = 0.45$.

The simulation initial conditions for the parameter vectors are $\theta_{f_1}(0) = \theta_{g_1}(0) = \theta_{f_2}(0) = \theta_{g_2}(0) = [0, \ldots, 0]^\top$, $\Psi_{f_1}(0) = \Psi_{g_1}(0) = \Psi_{f_2}(0) = \Psi_{g_2}(0) = [0.5, \ldots, 0.5]^\top$, and $\theta_{f_1}^0 = \theta_{g_1}^0 = \theta_{f_2}^0 = \theta_{g_2}^0 = [0, \ldots, 0]^\top$, $\Psi_{f_1}^0 = \Psi_{g_1}^0 = \Psi_{f_2}^0 = \Psi_{g_2}^0 = [0.005, \ldots, 0.005]^\top$. The adaptation rate matrices in (13-16) are set to $\Gamma_{f_1} = \Gamma_{g_1} = \Gamma_{f_2} = \Gamma_{g_2} = 30 I_N$, $\Gamma_{\Psi f_1} = \Gamma_{\Psi g_1} = \Gamma_{\Psi f_2} = \Gamma_{\Psi g_2} = 3 I_N$ where I_N is the identity matrix in $\Re^N$. For comparison purpose, we choose the same value for the σ parameter in simulations for each of the different modification terms. They are selected as $\sigma_{f_i} = \sigma_{g_i} = \frac{1}{300}$ and $\sigma_{\Psi f_i} = \sigma_{\Psi g_i} = \frac{1}{30}, i = 1, 2$.

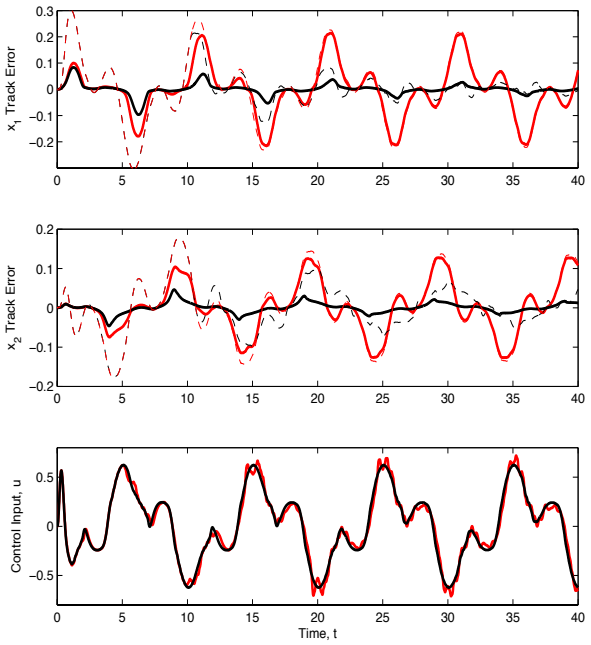

Fig. 3. Compensated tracking errors $\bar{x}_1$, $\bar{x}_2$, and the control input u for simulations (1) with adaptive bounding plus localized σ-modification (black solid lines) and standard σ-modification (red solid lines) for both θ_i and Ψ_i, and (2) without adaptive bounding (i.e., β terms are zero) plus localized (black dashed lines) and standard (red dashed lines) σ-modification algorithms for θ_i.

The control gains are selected as $k_1 = 2$ and $k_2 = 4$. In order to implement the $\omega(\cdot)$ function in the definitions of β_{f_i} and β_{g_i}, we select $\epsilon = 0.01$.

This example compares the compensated tracking error performance when the approximator parameter estimates and bounding parameter estimates are updated based on the adaptation laws of the three different modification methods. Figs. 3, 4 and 5 show the performance, over the first four repetitions of the reference trajectory, for the adaptation algorithms using σ-modification, $\bar{x}$-modification and deadzone modification, respectively. Each figure plots compensated tracking errors $\bar{x}_1$ (top), $\bar{x}_2$ (middle) and the control input u (bottom) for adaptation algorithms with localized (black lines) and standard (red lines) modification terms. To simplify the comparison between simulations with and without localization, we use the same approximator structure and the same design parameters.

The following discussion will first consider the results with adaptive bounding. The effect of global forgetting resulting from the standard modification terms is shown especially clearly in Fig. 3. Note that with the localized σ-modification (black solid curve), both $\bar{x}_1$ and $\bar{x}_2$ improve (i.e., become smaller) and the improvement is maintained when the trajectory revisits a subregion S_k

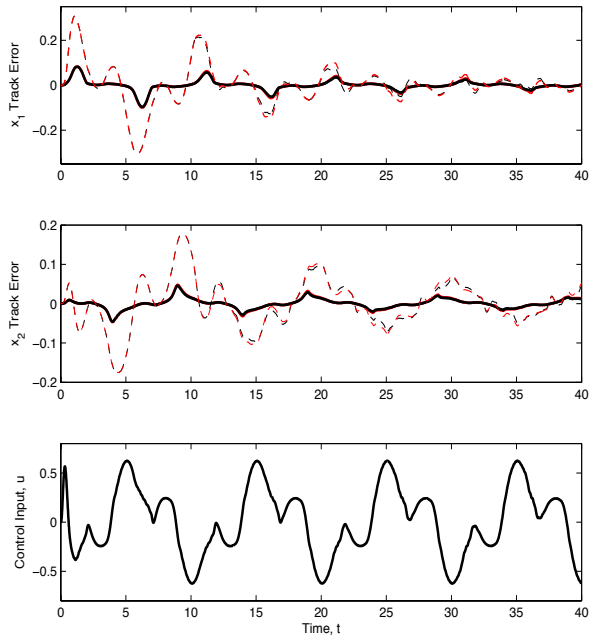

Fig. 4. Compensated tracking errors $\bar{x}_1$, $\bar{x}_2$, and the control input u for simulations (1) with adaptive bounding plus localized (black solid lines) and standard (red solid lines) $\bar{x}$-modification algorithms for both θ_i and Ψ_i, and (2) without adaptive bounding (i.e., β terms are zero) plus localized (black dashed lines) and standard (red dashed lines) $\bar{x}$-modification algorithms for θ_i.

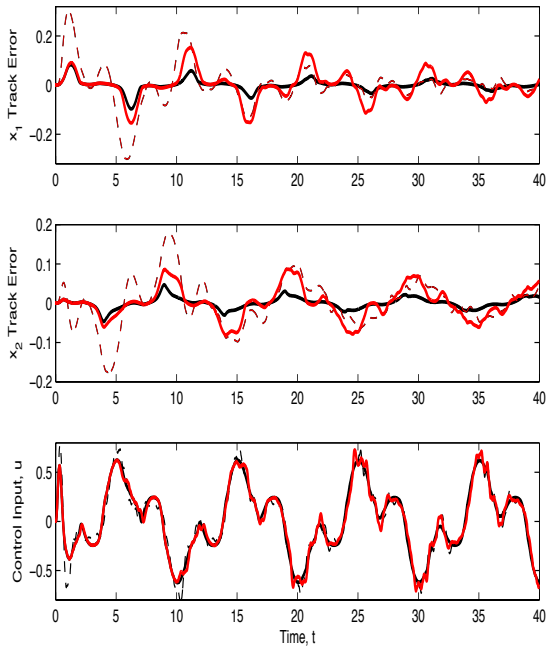

Fig. 5. Compensated tracking errors $\bar{x}_1$, $\bar{x}_2$, and the control input u for simulations (1) with adaptive bounding plus localized (black solid lines) and standard (red solid lines) deadzone modification algorithms for both θ_i and Ψ_i, and (2) without adaptive bounding (i.e., β terms are zero) plus localized (black dashed lines) and standard (red dashed lines) deadzone modification algorithms for θ_i.

of $\mathcal{D}$ where it has operated in the past. After initial transients, no improvement occurs for $\bar{x}_1$ or $\bar{x}_2$ when the standard σ-modification term is used. This is because the global effect of the σ-term causes the approximated functions and bounds to lose their local approximation accuracy on any subregion S_k of $\mathcal{D}$ when the trajectory leaves S_k. When the state returns to the same local region S_k later, all parameters will need to be estimated again. The adaptation laws with the localized σ-modification fix this issue by maintaining learned knowledge for later use, since the corresponding parameters relevant to S_k are left unchanged when the state is outside of S_k.

In Fig. 4, using the adaptation laws with the standard $\bar{x}$-modification terms (red solid) achieves improved (i.e., smaller) compensated tracking errors over each repetition of the reference trajectory. This indicates that a standard $\bar{x}$-modification term can be used to address the drifting in the parameter estimates when $x \in S_k$ and $\|\bar{x}\|$ is small. However, the parameter drifting could still occur for each parameter estimate when $x \notin S_k$, if $\|\bar{x}\|$ were not small. The localized $\bar{x}$-modification term is designed to address this issue by localizing the effect of drifting to the vicinity of the present operating point. Although we observe similar tracking performance for the standard $\bar{x}$-modification algorithm (red solid) and the localized $\bar{x}$-modification algorithm (black solid) in Fig. 4, these two algorithms have distinct learning features. When $x \notin S_k$, the parameter drifting caused by the standard $\bar{x}$-modification algorithm has a global effect, but at a much slower rate, than the standard σ-modification algorithm due to inclusion of the $\|\bar{x}\|$ term. Therefore, the local estimation accuracy could be mostly preserved in the standard $\bar{x}$-modification algorithm when the region is revisited later. The localized $\bar{x}$-modification algorithm can retain all knowledge learned from past experience for future use within S_k because the parameter drifting is localized to S_k and will not occur when $x \notin S_k$.

Fig. 5 has shown the tracking performance for simulations with the standard (red solid) and localized (black solid) deadzone modification algorithms. With the standard deadzone modification algorithm, we observe improvement for both $\bar{x}_1$ and $\bar{x}_2$ over each repetition of the reference trajectory. This is because the global forgetting caused by the standard deadzone modification will have no effect when $\|\bar{x}\|$ is small (i.e., within a designer specified deadzone). Therefore, local approximation accuracy on the subregion S_k is partially preserved for future use in the standard deadzone modification algorithm. Compared to tracking performance for the standard σ-modification algorithm (red solid) given in Fig. 3, the standard deadzone modification algorithm is shown to be effective to eliminate the issue of parameter drift-

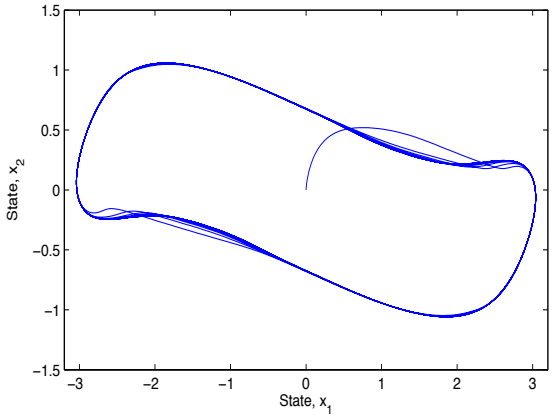

Fig. 6. Plot of x_2 versus x_1 for the simulation.

ing when $x \in S_k$ and $\|\bar{x}\|$ is small. However, the forgetting caused by the standard modification term will still have a global effect. Since the localized deadzone modification algorithm can address this issue and it will not lose any learned knowledge when $x \notin S_k$, better tracking performance is observed for the localized deadzone modification algorithm than for the standard deadzone modification algorithm in Fig. 5.

For simulations without adaptive bounding (i.e., β terms are all zero), we have also compared the tracking performance for localized (black dashed lines) and standard (red dashed lines) modification algorithms in Figs. 3, 4 and 5. In this case, only the approximator parameter estimates θ_i are updated based on either localized or standard modification algorithms, while the adaptation for the bounding parameter estimates Ψ_i is turned off. In Fig. 3, we observe the effect of global forgetting resulting from the standard σ-modification algorithm, while the localized σ-modification algorithm maintains improved (i.e., smaller) tracking error performance over each repetition of the reference trajectory. Similar comments about the $\bar{x}$-modification terms apply in Fig. 4 as were discussed for the case with adaptive bounding. Fig. 5 shows the same tracking error performance for localized (black dashed) and standard (red dashed) deadzone modification algorithms because the adaptation laws for θ_i for these two cases are the same.

The goal of this paragraph is to demonstrate the issue of global forgetting caused by the standard (i.e., non-localized) modification terms. To allow illustration of the approximator performance for a 2-input function, the figures will consider the true function and the approximated function versus x_1 for a fixed value of x_2 (i.e., $f_1(x_1, x_2)|_{x_2}$ and $\hat{f}_1(x_1, x_2)|_{x_2}$) at different times. Fig. 6 displays the x_1-x_2 trajectory from the simulation in a phase plane plot. Consider $x_2 = 0.27$, Fig. 6 shows that when x_2 is near 0.27 then, for the trajectory of this simulation, x_1 was either near $x_1 = -2.8$ or $x_1 \in [1.5, 2.5]$. Fig. 7 plots the true f_1 function (dotted) versus x_1 for $x_2 = 0.27$ and the approximation $\hat{f}_1(x_1, x_2)|_{x_2=0.27}$ at different simulation time instants when the adaptation algorithm is the localized σ-modification (top) and the standard σ-modification (bottom). It can be clearly seen that for x_2 near 0.27, the approximation $\hat{f}_1(x_1, x_2)$ is adapted near $x_1 = -2.8$ and for $x_1 \in [1.5, 2.5]$, but outside this x_1 range (e.g., near $x_1 = -0.5$) $\hat{f}_1(x_1, x_2)|_{x_2=0.27}$ stays near its initial value. This demonstrates locality of learning for both the local and global σ-modification methods. Fig. 7 also illustrates the different learning retention abilities between the local and global σ-modification methods. Fig. 7 shows the function approximation at $t = 0$s (solid), $t = 2$s (solid), $t = 105$s (dash-dot) and $t = 150$s (dashed). Consider the approximator plots at $t = 105$s to $t = 150$s. In the top subplot of Fig. 7 more accurate approximation is achieved at $t = 150$s than at $t = 105$s, which indicates that experience is accumulated and retained as time passes. When the standard σ-modification algorithm is used, the bottom subplot of Fig. 7 shows that the approximation accuracy that was achieved at $t = 105$s for $x_1 \in [1.5, 2.5]$ is lost at $t = 150$s. The function approximations for the other functions (i.e., f_2, g_1 and g_2) and the adaptive bounds behave similarly and are not given herein.

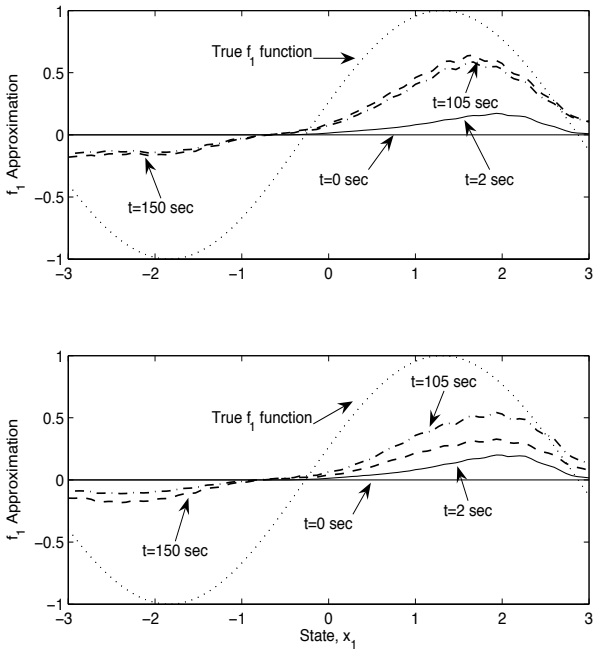

Fig. 7. True f_1 function (dotted) versus x_1 for $x_2 = 0.27$ and the approximation $\hat{f}_1$ at different times: $t = 0$s (solid), $t = 2$s (solid), $t = 105$s (dash-dot) and $t = 150$s (dashed)for the localized σmodification (top) and standard σ-modification (bottom).

7.7 Useful Properties

7.7.1 Discussion for Assumption 5

Assumption 5 *The scalar function* $-1 \leq \omega(z) \leq 1$ *satisfies*

$$0 \leq |z| - z\omega\left(\frac{z}{\epsilon}\right) \leq \eta\epsilon \quad \forall z \in \Re, \tag{66}$$

for any $\epsilon > 0$ *and some constant* $0 < \eta < \infty$.

The function $\omega(z) = tanh(z)$ satisfies Assumption 5 for η satisfying $\eta = e^{-(\eta+1)}$, i.e. $\eta = 0.2785$ (Polycarpou 1996). The function

$$\omega(z) = \text{sat}(z) = \begin{cases} 1 & \text{for} \quad z \geq 1 \\ z & \text{for} \quad |z| \leq 1 \\ -1 & \text{for} \quad z \leq -1. \end{cases}$$

satisfies Assumption 5 with $\eta = 0.25$.

The inequality (66) in Assumption 5 can be extended to another form needed in Section 5. The bound

$$0 \leq |z| - z\omega\left(\frac{z_a}{\epsilon}\right) \leq \left|\frac{z}{z_a}\right| \eta\epsilon \tag{67}$$

will be used to address the case of $z_a \neq z$, but $sign(z_a) = sign(z)$.

The inequality (67) can be shown by multiplying both sides of

$$0 \leq |z_a| - z_a\omega\left(\frac{z_a}{\epsilon}\right) \leq \eta\epsilon$$

by $\left|\frac{z}{z_a}\right|$. After algebraic manipulations, we have

$$0 \leq |z| - sgn(z_a)|z_a|\left|\frac{z}{z_a}\right|\omega\left(\frac{z_a}{\epsilon}\right) \leq \left|\frac{z}{z_a}\right|\eta\epsilon$$

$$0 \leq |z| - sgn(z)|z|\omega\left(\frac{z_a}{\epsilon}\right) \leq \left|\frac{z}{z_a}\right|\eta\epsilon$$

which completes the proof.

7.7.2 Adaptation Law with Parameter Projection

The objective of this appendix is to derive convex sets within which the parameter updates of θ_{gi} and $\Psi_{gi}, i = 1, \ldots, n$ can be constrained to ensure that $\hat{g}_i + \beta_{g_i}$ satisfies the controllability condition of Assumption 3.

For controllability, we must have $\hat{g}_i + \beta_{g_i} > g_l$ which is the same as

$$\theta_{g_i}^\top \Phi_{g_i} + \Psi_{g_i}^\top \Phi_{g_i}\omega(\cdot) > g_l, \ i = 1, \ldots, n \tag{68}$$

where the argument dependence of the function ω is dropped for presentation simplicity. Since $-1 \leq \omega(\cdot) \leq 1$, we can show

$$-\Psi_{g_i}^\top \Phi_{g_i} \leq \Psi_{g_i}^\top \Phi_{g_i}\omega(\cdot) \leq \Psi_{g_i}^\top \Phi_{g_i}. \tag{69}$$

Therefore, it is easy to see that inequality (68) will hold $\forall x \in \mathcal{D}$ if and only if

$$\theta_{g_i}^\top \Phi_{g_i}(x) - \Psi_{g_i}^\top \Phi_{g_i}(x) > g_l, \ \forall x \in \mathcal{D}, \ i = 1, \ldots, n. \tag{70}$$

If the $\Phi_{g_i}, 1 \leq i \leq n$ form a partition of unity (i.e., $\sum_j \Phi_{g_i,j} = 1$), we can easily show that condition (70) is satisfied if and only if, for any $x \in \mathcal{D}$ and $i = 1, \ldots, n, j = 1, \ldots, N$,

$$\theta_{g_i,j} > g_l, \ 0 \leq \Psi_{g_i,j} < \theta_{g_i,j} - g_l \tag{71}$$

is satisfied. The reason why we prefer to use condition (71) instead of condition (70) is that the condition (71) defines a convex set within which the projection modification can be easily applied.

Then, we use the following parameter projection to constrain the parameter updates

$$P_S\{\dot{\theta}_{g_i,j}\} = \begin{cases} \dot{\theta}_{g_i,j} & \text{if } \theta_{g_i,j} > g_l \text{ or } \dot{\theta}_{g_i,j} > 0 \\ 0 & \text{otherwise.} \end{cases} \tag{72}$$

Similarly,

$$P_S\{\dot{\Psi}_{g_i,j}\} = \begin{cases} \dot{\Psi}_{g_i,j} & \text{if } \left(\Psi_{g_i,j} < \theta_{g_i,j} - g_l \text{ or } \dot{\Psi}_{g_i,j} < 0\right) \\ & \text{and } \left(\Psi_{g_i,j} > 0 \text{ or } \dot{\Psi}_{g_i,j} > 0\right) \\ 0 & \text{otherwise.} \end{cases}$$

7.7.3 Proof of Lemma 1

Proof: Since the function M is positive definite and satisfies the inequality

$$\frac{d}{dt}M(\mathbf{z}, \Theta_1, \cdots, \Theta_p, t) \leq -c_1\|\mathbf{z}\|^2 + c_2,$$

we know that $\dot{M}$ is negative definite whenever $c_1\|\mathbf{z}\|^2 > c_2$. Assume that $\|\mathbf{z}(t)\| > \sqrt{\frac{c_2}{c_1}}$ for $t \in (\tau_1, \tau_2)$. Therefore, the function $M(\mathbf{z}, \Theta_1, \cdots, \Theta_p, t)$ on (τ_1, τ_2) is bounded by $M(\mathbf{z}, \Theta_1, \cdots, \Theta_p, \tau_1)$.

Let $t \in [\tau_2, \tau_3]$ with $\|\mathbf{z}(t)\| \leq \sqrt{\frac{c_2}{c_1}}$, we will next show that each $\Theta_i(t)$ is bounded on $[\tau_2, \tau_3]$. Since Θ_i satisfies

$$\dot{\Theta}_i = \frac{d}{dt}(\Theta_i - \Theta_i^0) = \Gamma[\Phi z_i - c_0 R(\Theta_i - \Theta_i^0)],$$

Then $\Theta_i(t)$ can be explicitly solved as

$$\Theta_i(t) = \Theta_i^0 + \Big(\Theta_i(\tau_2) - \Theta_i^0\Big) e^{-c_0\Gamma \int_{\tau_2}^{t} R(\mathbf{z}(\lambda))d\lambda} + \int_{\tau_2}^{t} e^{-c_0\Gamma \int_{\lambda}^{t} R(\mathbf{z}(v))dv} \Gamma\Phi(\mathbf{z}(\lambda)) z_i(\lambda) d\lambda.$$

Note that for $t \in [\tau_2, \tau_3]$, $|z_i(t)| \leq \sqrt{\frac{c_2}{c_1}}$, $R(\mathbf{z})$ is a square diagonal matrix with nonnegative diagonal components, and $\Phi(\mathbf{z})$ is a vector of positive, bounded functions; therefore, $\|\Theta_i(t)\|$ is bounded on $[\tau_2, \tau_3]$ by a finite value, i.e., there exists a $\bar{\Theta}_i$ such that

$$\|\Theta_i(t)\| < \bar{\Theta}_i < \infty.$$

Also, it is easy to show that M is bounded such that $M(\mathbf{z}, \Theta_1, \cdots, \Theta_p, t) < \varphi_2\left(\sqrt{\frac{c_2}{c_1}}, \bar{\Theta}_1, \cdots, \bar{\Theta}_p\right) < \infty$ for $t \in [\tau_2, \tau_3]$.

We thus conclude the boundedness of $M(\mathbf{z}, \Theta_1, \cdots, \Theta_p)$, $|z_i(t)|$ and $\|\Theta_i(t)\|$ for any $t \in [0, t_f]$. ■

7.7.4 Proof of Theorem 1

Proof. When $x \notin \mathcal{D}$, we have already shown in Section 7.3 that the sliding components $u_{s_i}, i = 1, \ldots, n$ will return the state to $\mathcal{D}$ in finite time.

The proof for the case of $x \in \mathcal{D}$ and $\delta_{f_i} = \delta_{g_i} = 0$ is based on the eqn. (21). The negative semi-definiteness of $\frac{dV}{dt}$ implies that the variables $\bar{x}_i, \theta_{f_i}, \theta_{g_i}, i = 1, \ldots, n$ are each bounded. Let $Z(t) = \|\bar{x}(t)\|^2$. Since $\int_0^\infty Z(\tau)d\tau \leq \frac{V(0)}{\underline{k}} < \infty$ and $\dot{Z}(t) = \sum_{i=1}^n \bar{x}_i \dot{\bar{x}}_i$ is bounded, Barbalat's lemma (p. 123 in (Slotine & Li, 1991)) applied to $Z(t)$ implies that each $\bar{x}_i$ approaches zero as t approaches infinity. Finally, since

$$\begin{aligned} \dot{V} &\leq -\sum_{i=1}^{n} k_i \bar{x}_i^2 \\ V(t) - V(0) &\leq -\sum_{i=1}^{n} \int_0^t k_i \bar{x}_i^2(\tau) d\tau \\ V(0) &\geq \sum_{i=1}^{n} \int_0^t k_i \bar{x}_i^2(\tau) d\tau, \end{aligned} \tag{73}$$

we show that each $\bar{x}_i$ is in $\mathcal{L}_2$. ■

7.7.5 Proof of Theorem 2

Proof. For the proof herein, we only consider the case of $x \in \mathcal{D}$. When $x \notin \mathcal{D}$, we have already shown in Section 7.3 that sliding control terms we define will return the state to $\mathcal{D}$.

Using Lemma 1, we have that $V(t)$ defined in (17) is bounded and then $\bar{x}_i, \tilde{\theta}_{f_i}, \tilde{\theta}_{g_i}, \tilde{\Psi}_{f_i}, \tilde{\Psi}_{g_i} \in \mathcal{L}_\infty$. This yields directly $\theta_{f_i}, \theta_{g_i}, \Psi_{f_i}, \bar{\Psi}_{g_i} \in \mathcal{L}_\infty$. The fact that $x_i \in \mathcal{L}_\infty$ comes from the fact that x_d and ξ_i are bounded.

Together with the boundedness of Φ_{f_i} and Φ_{g_i}, we can show directly that $u \in \mathcal{L}_\infty$ and then $\dot{\bar{x}}_i$, $\dot{\theta}_{f_i}$, $\dot{\theta}_{g_i}$, $\dot{\Psi}_{f_i}$, $\dot{\Psi}_{g_i} \in \mathcal{L}_\infty$.

For the proof of Item 4 given by (30), we consider integrating (28) on both sides to obtain

$$\begin{aligned} V(t+T) - V(t) &\leq \int_t^{t+T} (-\underline{k}\|\bar{x}(\tau)\|^2 + \bar{d} + \rho_1) d\tau \\ \underline{k} \int_t^{t+T} \|\bar{x}(\tau)\|^2 \, d\tau &\leq V(t) + \int_t^{t+T} (\bar{d} + \rho_1) d\tau \end{aligned}$$

which directly yields (30). ■

7.7.6 Proof of Theorem 3

Proof. Properties 1, 2, 3 of Theorem 3 are straightforward to show given the form of inequality (52). The proof is similar to the proof of Theorem 2 in Section 5.1 and will not be repeated here.

Property 4 can be proved by integrating on both sides of (52) as

$$\begin{aligned} V(t+T) - V(t) &\leq \int_t^{t+T} (-\frac{1}{2}\underline{k}\|\bar{x}(\tau)\|^2 + \bar{d} + \rho_2) d\tau \\ \frac{\underline{k}}{2} \int_t^{t+T} \|\bar{x}(\tau)\|^2 \, d\tau &\leq V(t) + \int_t^{t+T} (\bar{d} + \rho_2) d\tau \end{aligned}$$

which directly yields (54). ■

7.7.7 Proof of Theorem 4

Proof. Substituting the Q terms defined in (55–58) into (22), for $x \in \mathcal{D}$ and $\|\bar{x}\| > \sqrt{\frac{\bar{\rho}_3 + \mu}{\underline{k}}}$, $\dot{V}$ is written as

$$\begin{aligned} \dot{V} \leq & -\underline{k}\|\tilde{x}\|^2 + \bar{d} \\ & - \sum_{i=1}^{n} \Big(\sigma_{\Psi f i} \tilde{\Psi}_{f_i}^\top R_{f_i} (\Psi_{f_i} - \Psi_{f_i}^0) \\ & \quad + \sigma_{\Psi g i} \tilde{\Psi}_{g_i}^\top R_{g_i} (\Psi_{g_i} - \Psi_{g_i}^0) \Big). \end{aligned}$$

Similarly as in Section 5.1, we obtain

$$\dot{V} \leq -\underline{k}\|\bar{x}\|^2 + \bar{d} + \rho_3 \tag{74}$$

$$\leq -\underline{k}\|\tilde{x}\|^2 + \bar{\rho}_3 \leq -\mu < 0. \tag{75}$$

where ρ_3 is defined in eqn. (59). Therefore, if $\|\bar{x}\| > \sqrt{\frac{\bar{\rho}_3 + \mu}{\underline{k}}}$, then V is decreasing. If $\|\bar{x}\| \leq \sqrt{\frac{\bar{\rho}_3 + \mu}{\underline{k}}}$ then

$\tilde{\theta}_{f_i}, \tilde{\theta}_{g_i}, \tilde{\Psi}_{f_i}$ and $\tilde{\Psi}_{g_i}, i = 1, \ldots, n$ are all constant and $\|\bar{x}\|$ is bounded. Thus, $V(t)$ is bounded by the maximum of $V(0)$ or

$$\max_{\|\bar{x}\|=\sqrt{\frac{\bar{\rho}_3+\mu}{\underline{k}}}} \Big(V(\bar{x}, \tilde{\theta}_{f_i}(0), \tilde{\theta}_{g_i}(0), \tilde{\Psi}_{f_i}(0), \tilde{\Psi}_{g_i}(0))\Big)$$

which shows that $\bar{x}_i, \tilde{\theta}_{f_i}, \tilde{\theta}_{g_i}, \tilde{\Psi}_{f_i}, \tilde{\Psi}_{g_i} \in \mathcal{L}_\infty$. Properties 2, 3 of Theorem 4 can be similarly shown.

For the proof of Item 4, we integrate (74) to obtain

$$\begin{aligned}
\underline{k} \int_t^{t+T} \|\tilde{x}(\tau)\|^2 d\tau &\leq V(t) + \int_t^{t+T} (\bar{d} + \rho_3) d\tau \\
\int_t^{t+T} \|\tilde{x}(\tau)\|^2 d\tau &\leq \frac{1}{\underline{k}} V(t) + \frac{1}{\underline{k}} \bar{\rho}_3 T \\
&\leq \frac{1}{\underline{k}} V(t) + b_d^2 T
\end{aligned}$$

which implies $\bar{x}$ is small in the mean square sense (m.s.s.).

Next, we will show Property 5 using a method of proof similar to that in Chapter 1 of (French *et al.*, 2003). Assume x starts outside the deadzone at t_0, enters the deadzone at t_{2i-1} and leaves it at t_{2i}, for $i \geq 1$. Then, at the boundary of deadzone

$$V(t_{2i-1}) = V(t_{2i}),$$

in the deadzone

$$V(t) \leq V(t_{2i-1}), \forall t \in [t_{2i-1}, t_{2i}],$$

and outside the deadzone according to (75),

$$V(t_{2i+1}) - V(t_{2i}) < -\mu(t_{2i+1} - t_{2i}).$$

Therefore, the total time of x staying outside the deadzone is

$$T_d = (t_1 - t_0) + \sum_{i \geq 1} (t_{2i+1} - t_{2i}),$$

and

$$\begin{aligned}
T_d &< \frac{1}{\mu}\Big(V(t_0) - V(t_1) + \sum_{i \geq 1} (V(t_{2i}) - V(t_{2i+1}))\Big) \\
&< \frac{1}{\mu}\Big(V(t_0) - V(t_1) + \sum_{i \geq 1} (V(t_{2i-1}) - V(t_{2i+1}))\Big) \\
&< \frac{V(t_0)}{\mu}
\end{aligned}$$

which is a finite value. ■